Fractal Dimension of Resting-State EEG as a Biomarker for Autonomous Sensory Meridian Response (ASMR)

Shyamal Y. Dharia, Camilo E. Valderrama, *Member, IEEE*, Qian Liu, *Member, IEEE*, Beverley K. Fredborg, Amy S. Desroches, and Stephen D. Smith

***Abstract*—Autonomous Sensory Meridian Response (ASMR) is an audio-visual phenomenon characterized by multisensory experiences in response to specific auditory stimuli, typically triggering a tingling sensation beginning in the scalp and neck and accompanied by decreased heart rate and deep relaxation. While prior electroencephalogram (EEG) studies have identified ASMR-related neural signatures in stimulus-based paradigms, resting-state differences between ASMR-sensitive (ASMR+) and non-sensitive (ASMR-) individuals remain unexplored. In this study, we apply Higuchi's fractal dimension (HFD) to eyes-open and eyes-closed resting-state EEG and demonstrate that ASMR+ participants exhibit significantly lower complexity in the delta (1–4Hz) and theta (4–8Hz) bands and higher complexity in the alpha (8–12Hz) band. Moreover, we train Transformer, Mamba, Random Forest and SVM classifiers on these HFD features to distinguish ASMR+ individuals from ASMR-, achieving F1 scores of 82.56% , 77.33% , 73.93% , and 70.85% , respectively. Finally, using an explainable-AI approach, we showed that ASMR+ participants had significantly lower hubness proportions (network connectivity) than ASMR-. These findings reveal novel resting-state biomarkers of ASMR sensitivity and lay the groundwork for rapid, noninvasive EEG-based screening in ASMR-augmented therapeutic applications. The code has been released on https://github.com/Shyamal-Dharia/Fractal-Dimension-of-Resting-State-EEG-as-a-Biomarker-for-Autonomous-Sensory-Meridian-Response-ASMR- GitHub.**

***Index Terms*—Autonomous sensory meridian response (ASMR), electroencephalography (EEG), resting-state EEG.**

I. Introduction

AUTONOMOUS Sensory Meridian Response (ASMR) is a perceptual phenomenon in which specific auditory and visual stimuli elicit a tingling sensation that typically starts in the scalp and neck and can spread down the spine and limbs [1]. These somatosensory "tingles" are accompanied by measurable physiological changes, heartrate deceleration and increased skin conductance, and are reliably associated with positive affect and deep relaxation [1], [2]. Unlike frisson "chills," which are sporadic and stimulusdependent, ASMR sensations can be anticipated by individuals who learn which cues—whispered speech, gentle tapping, slow repetitive tasks, etc.—consistently trigger them [3]. Recent work comparing ASMR with other atypical sensory experiences further suggests that ASMR relies on a distinct pattern of neural activation [4]. These differential brain activations may support the more pronounced relaxation and heart-rate deceleration observed in those who experience ASMR, suggesting that ASMR stimuli can induce deeper states of relaxation in sensitive individuals.

The physiological relaxation and feeling of calmness associated with ASMR suggest that it may provide psychological benefits to some individuals. Indeed, survey studies of ASMR-sensitive (ASMR+) individuals indicate that many people use ASMR-eliciting videos as a method of decreasing stress and symptoms of depression [1]. Given that roughly one adult in five reports being ASMR+ [5], [6] and approximately 35.1% of respondents in a Gallup World Poll report experiencing substantial daily stress, the potential clinical benefits of ASMR are immense. Specifically, it is likely that ASMR-based interventions could serve as a supplement to conventional therapies such as cognitive behavioral therapy. A limiting factor in incorporating ASMR into clinical interventions is identifying whether an individual is ASMR+. Currently, clinicians must rely on subjective

Received 20 May 2025; revised 19 August 2025; accepted 14 September 2025. This work was supported in part by Natural Sciences and Engineering Research Council of Canada (NSERC) Discovery under Grant RGPIN-2023-03443, Grant RGPIN-2024-05844, and Grant RGPIN-2024-05575, in part by operating costs from the NSERC under Grant 418650-2012, in part by infrastructure support from the Canada Foundation for Innovation John Evans Leadership Fund under Grant 31560, and in part by the Manitoba Medical Service Foundation under Grant 2025-03. *(Corresponding author: Stephen D. Smith.)*

This work involved human subjects or animals in its research. Approval of all ethical and experimental procedures and protocols was granted by University of Winnipeg Human Research Ethics Board Application No. B2014:078, and performed in line with the ethical requirements of Tri-Council Policy Statement: Ethical Conduct for Research Involving Humans (TCPS 2).

Shyamal Y. Dharia is with the Department of Applied Computer Science, The University of Winnipeg, Winnipeg, MB R3B 2E9, Canada (e-mail: s.dharia-ra@uwinnipeg.ca).

Camilo E. Valderrama is with the Department of Applied Computer Science, The University of Winnipeg, Winnipeg, MB R3B 2E9, Canada, and also with the Department of Community Health Sciences, Cumming School of Medicine, University of Calgary, Calgary, AB T2N 4Z6, Canada (e-mail: c.valderrama@uwinnipeg.ca).

Qian Liu is with the Department of Applied Computer Science, The University of Winnipeg, Winnipeg, MB R3B 2E9, Canada, and also with the Department of Biochemistry and Medical Genetics, Max Rady College of Medicine, University of Manitoba, Winnipeg, MB R3E 0J9, Canada (e-mail: qi.liu@uwinnipeg.ca).

Beverley K. Fredborg, Amy S. Desroches, and Stephen D. Smith are with the Department of Psychology, The University of Winnipeg, Winnipeg, MB R3B 2E9, Canada (e-mail: b.fredborg@uwinnipeg.ca; a.desroches@uwinnipeg.ca; s.smith@uwinnipeg.ca).

Digital Object Identifier 10.1109/JBHI.2025.3612301

screening questions (e.g. "Do you experience ASMR tingles?"); such measures are prone to demand characteristics and recall bias, particularly in clinical populations. To overcome these limitations, our study aims to identify an objective biomarker from a brief, stimulusfree restingstate EEG. By distinguishing ASMR- from ASMR+ individuals at rest, this neural metric could enable accurate screening, guide personalized ASMR protocols, and facilitate integration of ASMR into clinical practice.

Prior research has sought to characterize ASMR-related neural patterns using neuroimaging modalities such as functional MRI (fMRI) and electroencephalography (EEG) [4], [7], [8]. For instance, Smith et al. [4], using resting-state fMRI, demonstrated that individuals with ASMR exhibit weaker and less distinct resting-state brain network connectivity than ASMR- individuals. However, while fMRI has high spatial resolution, its cost and limited availability make it impractical for frequent assessments. In contrast, EEG offers a more accessible alternative: Engelbregt et al. [9] reported that ASMR stimuli can reduce depressive symptoms in ASMR+ individuals and lower heart rates across all participants, regardless of ASMR sensitivity. Additionally, Ohta et al. [10] showed that ASMR exposure mitigates mental stress during cognitively demanding tasks, as evidenced by a significant drop in alpha-band power alongside an increase in beta-band power. Collectively, these studies provide valuable insights into the potential of ASMR stimuli to alleviate stress, lower physiological arousal, and reveal unique neural activity patterns.

Although several studies have characterized the acoustic structure of ASMR triggers (e.g., Tan et al. [11]) and others have developed deeplearning platforms to generate ASMR content (e.g., DeepASMR [12]), to our knowledge, no prior work has attempted to detect, using machine learning, whether an individual is ASMR+ from restingstate EEG data. Because ASMR sensitivity is unique and has traitlike differences in how the brain processes sensory input, we hypothesized that these trait-like differences would also be reflected in the brain's spontaneous resting-state activity. Indeed, using fMRI, Smith et al. [4] observed that ASMR was linked to reduced functional connectivity in the salience and visual networks, as well as unusual connectivity patterns in the default mode, central executive, and sensorimotor networks.

To that extent, the present study aims to identify novel resting-state EEG features associated with ASMR+ individuals. Rather than using power-spectrum analysis, which assumes that EEG is time-invariant and fails to capture its non-linear fluctuations, we use Higuchi's fractal dimension (HFD) [13]. HFD is a single scalar, monofractal index of signal complexity that quantifies how irregular the waveform is when examined at both fast and slow time intervals. Furthermore, we explored whether machine learning models trained on HFD features can accurately classify ASMR- and ASMR+ individuals. To our knowledge, this is the first study to apply EEG-based fractal dimension analysis combined with machine learning classification to differentiate ASMR sensitivity, thus laying essential groundwork for future AI applications for ASMR.

II. Related Work

A. Neural Signatures of ASMR

Early resting-state fMRI work revealed that the *default-mode network* (DMN) of ASMR+ individuals shows significantly less connectivity than ASMR- [14]. Extending this observation, Smith et al. [4] examined five canonical resting-state networks (DMN, salience, central–executive, sensorimotor, and visual) and confirmed a global pattern of reduced within-network connectivity together with heightened orbitofrontal–sensorimotor coupling—an arrangement interpreted as a substrate for the rewarding "tingle" experience. Another fMRI study showed that subjects who experienced ASMR while watching ASMR videos showed significant activation in regions associated with both reward and emotional arousal [15]. Additionally, Smith et al. [16] found that ASMR videos elicit activity in brain areas related to sensation, emotion, and attention in ASMR+ individuals, but not in matched ASMR- participants. Together, these findings indicate that ASMR is grounded in both atypical large-scale connectivity at rest and the transient co-activation of reward, sensation, attention and emotional arousal during stimulation.

Fredborg et al. [7] conducted the first EEG study of ASMR using both auditory and audiovisual stimuli and showed that ASMR triggers enhance frontal alpha (8–12 Hz) power, reflecting a relaxed, flow-like attentional state, and boost sensorimotor-rhythm (12–15 Hz) and gamma ($>$ 30Hz) activity over primary sensorimotor cortices, consistent with the characteristic tingling sensation. Mohammadi et al. [8] later extended these results using a similar video paradigm, reporting a global reduction in delta (1–4Hz) power alongside elevated occipital alpha and increased left fronto-temporal beta (12–30Hz) power during ASMR viewing. Both studies, therefore, converge on alpha amplification as a robust electrophysiological marker of ASMR, while implicating higher-frequency rhythms in sensorimotor and fronto-temporal regions in encoding the tingling component of the experience.

However, these prior EEG studies neither explored resting-state conditions with eyes open versus closed nor went beyond power-spectrum analysis, which, while informative, offers limited insight into the temporal complexity of neural signals. In contrast, fractal-dimension metrics such as the HFD have uncovered unique EEG dynamics in other contexts. For example, theta binaural-beat stimulation elicited a significant decrease in HFD within temporal and parietal lobes in just three minutes—about half the time required to detect comparable changes in spectral power—demonstrating HFD's sensitivity to rapid brain entrainment [17]. Another study reported that patients with diffuse axonal injury exhibited the highest resting-state fractal dimensions, underscoring HFD's potential for clinical neurodiagnostics [18]. Although many EEG studies have applied HFD, none have used it to characterize ASMR neural signatures. To address this gap, we investigate HFD features to identify the neural correlates of ASMR and to assess whether these features can accurately distinguish ASMR+ individuals from ASMR- using machine learning.

III. Methods

A. Dataset and Participants

Thirty-one University of Winnipeg students participated in our EEG study: sixteen in the ASMR+ group and fifteen in the ASMR- group (see Table I). Participants were initially classified as being ASMR+ or ASMR- based on self-reports of their previous perceptual experiences. To confirm this classification, all participants viewed two ASMR-eliciting videos on YouTube.com while being interviewed by a psychologist

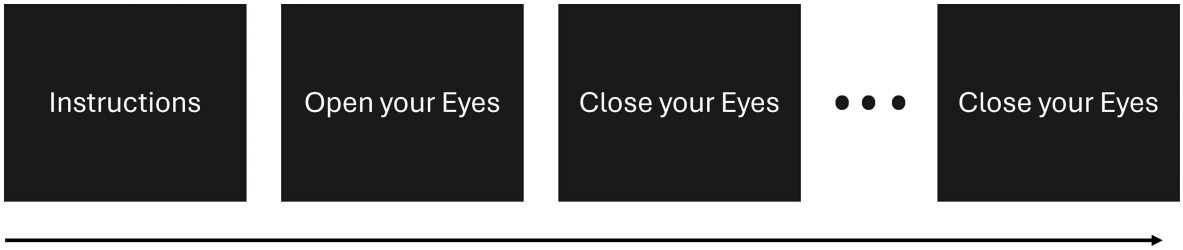

Fig. 1. Experimental protocol. Participants were informed that the study aimed to measure baseline neural activity during alternating eyes-open and eyes-closed resting-state conditions. The fixed sequence for all participants was: OPEN–CLOSED–OPEN–CLOSED–OPEN–CLOSED, with each condition repeated three times for one minute each.

TABLE I
PARTICIPANT DEMOGRAPHICS BY GROUP

Group	N	Female	Male	Age ($\mu \pm \sigma$)
ASMR-	15	9	6	23.87 ± 4.81
ASMR+	16	10	6	23.94 ± 4.58
Overall	**31**	**19**	**12**	$\mathbf{23.90 \pm 4.61}$

from the research team. During this interview, participants were asked to describe their sensory and emotional responses. All ASMR+ participants reported experiencing tingling sensations; ASMR "tingles" were not reported by any ASMR- individual. All participants also completed the ASMR Checklist [14] to identify the specific stimuli that triggered ASMR. However, due to the fact that all participants reported being sensitive to the same ASMR triggers (i.e., all participants reported "whispering" as a primary trigger), data from the ASMR Checklist did not distinguish between participants and was therefore excluded from subsequent analyses. EEG signals were recorded with a 31-channel Ag/AgCl EasyCAP (Brain Products), sampled at 500 Hz using BrainVision Recorder, and amplified via the actiCHamp system. Throughout the recording, electrode impedances were kept less than 20 kΩ.

All subjects signed informed consent forms before participation and earned course credits. The University of Winnipeg Psychology Department's Research Ethics Committee approved this study under code PSYREB-2015-520. Therefore, all required steps of this study followed our institutional rules, national ethics guidelines, and the principles of the 1964 Helsinki Declaration and its subsequent amendments. A detailed description of the experimental procedure is provided in Fig. 1.

B. EEG Preprocessing

The EEG preprocessing pipeline involved several stages. First, raw signals originally sampled at 500 Hz were downsampled to 250 Hz to reduce computational overhead. A 1 Hz high-pass filter was applied to remove slow drifts, followed by a 60 Hz notch filter to suppress power line noise. To remove ocular artifacts, specifically eyeblinks and horizontal saccades, we performed Independent Component Analysis (ICA) using the HEOG and VEOG channels. We applied MNEPython to perform ICA with correlation as a measure to identify components that exceed a Pearson correlation of 0.9 to flag and remove artifact components. Given that filtering is a linear operation, the ICA decomposition obtained from the filtered data was applied to the unfiltered but downsampled signal, following the approach of Winkler et al. [19]. ICA components associated with ocular artifacts were then removed from this unfiltered dataset. Subsequently, a band-pass filter (1–45 Hz) was applied, in order to exclude both low-frequency drifts and high-frequency noise. Also, it is to be noted that we dropped HEOG and VEOG channels and only used EEG channels for further analysis. Finally, the data were separated into segments corresponding to eyes-open and eyes-closed conditions for condition-specific analyses.

C. Statistical Analysis

For statistical analysis, we first bandpass filtered each one-minute segment of raw EEG data (15,000 samples per segment at 250 Hz) into the five standard frequency bands: delta (1–4 Hz), theta (4–8 Hz), alpha (8–12 Hz), beta (12–30 Hz), and gamma (30–45 Hz). We then extracted HFD values per subject, segment, channel, and band—following equations 1, 2, and 3—to measure signal complexity. This yields a data matrix of size: 31 subjects × 6 segments × 31 channels × 5 frequency bands. To avoid assumptions of normality, we used the Wilcoxon rank-sum test, a non-parametric method, for statistical comparisons. Testing was conducted at two spatial aggregation levels: (i) five cortical regions and (ii) individual EEG channels. For the regional analysis, five frequency bands across five regions yielded 25 comparisons per feature and a total of 50 tests (25 for the eyes-open condition and 25 for the eyes-closed condition). Separately, for the channel-wise analysis, Wilcoxon rank-sum tests were performed for all 31 channels and five frequency bands, resulting in 155 comparisons per feature and a total of 310 tests (155 for eyes-open and 155 for eyes-closed). To control for multiple comparisons across both the region-based and channel-based analyses, we applied the Benjamini–Hochberg False Discovery Rate (FDR) correction separately within each set of p-values.

D. Feature Extraction

For machine learning, each subject's sixminute EEG recording (three minutes eyesopen, three minutes eyesclosed) was segmented into nonoverlapping 10 s windows, yielding eighteen windows per condition and thirtysix windows per subject. We segmented the data to provide our classifiers with enough observations to learn diverse EEG patterns. For each 10 s window, we computed HFD across $C = 31$ EEG channels and $F = 5$ frequency bands, resulting in a threedimensional feature matrix of size $N \times C \times F$, where $N = 36$ windows per subject. Across our cohort of $S = 31$ subjects, this yielded a total of $S \times N = 31 \times 36 = 1116$ samples, corresponding to 558 samples per condition.

The HFD was computed using Higuchi's algorithm, which estimates the fractal dimension D of a time series $X = \{x(1), x(2), \ldots, x(N)\}$ by constructing k-length subsequences and evaluating their average length $L(k)$ (Equations1–3). In our implementation, we set $k_{\max} = \lfloor N/2 \rfloor$, so that the maximum interval between points spans half the segment while still using the full data for each calculation. The full set of interval lengths k is then drawn in $\log_2$-space from 2 up to $k_{\max}$, and the fractal dimension D is estimated as the slope of the linear fit in the $(\log k, \log L(k))$ space.

$$L_m(k) = \frac{1}{\lfloor \frac{N-m}{k} \rfloor k} \sum_{i=1}^{\lfloor \frac{N-m}{k} \rfloor} \left| x(m + i\,k) - x(m + (i-1)\,k) \right|, \tag{1}$$

$$L(k) = \frac{1}{k} \sum_{m=1}^{k} L_m(k), \tag{2}$$

$$D = \text{slope of the linear fit of } \log L(k) \text{ vs. } \log k. \tag{3}$$

Finally, we applied *min–max normalization* to each subject's features:

$$X' = \frac{X - X_{\min}}{X_{\max} - X_{\min}},$$

where $X_{\min}$ and $X_{\max}$ are the minimum and maximum values over all samples for that subject.

E. Network Architectures

We utilized two neural network architectures in our pipeline—Transformers [20] and Mamba [21]—to learn spatial representations from EEG data. We adopted the vanilla versions of both models, originally designed for temporal sequence modeling, and repurposed them for spatial feature learning.

Transformers: In our setup, we treat EEG channels as sequence positions and their corresponding feature vectors as embeddings. Concretely, for a batch of size B, with C EEG channels and $F = 5$ HFD features per channel, our input tensor has shape (B, C, F). The core mechanism of transformers is Multi-Head Attention (MHA) that computed via scaled dotproduct attention:

$$\text{Attention}(Q, K, V) = \text{softmax}\left(\frac{QK^T}{\sqrt{d_k}}\right) V \tag{4}$$

where $Q, K, V \in \mathbb{R}^{C \times d_k}$ are learned linear projections of the channel-wise feature embeddings, and d_k represents the dimension of the K vectors. By running several such heads in parallel, MHA captures rich, long-range spatial dependencies across channels and frequency bands. Moreover, the attention weight matrix

$$\text{softmax}\big(QK^\top / \sqrt{d_k}\big) \tag{5}$$

can be visualized to reveal which EEG channels the model focuses on when making its predictions.

Mamba: We repurposed Mamba—originally a State Space Model (SSM)-based temporal model—for spatial modeling of EEG by treating each electrode index as a "time" step. Its core state-space recursion is

$$x_{c+1} = A\,x_c + B\,u_c, \qquad y_c = C\,x_c, \tag{6}$$

Algorithm 1: Transformer-Attention Hubness.

Input: Attention maps $A \in \mathbb{R}^{T \times C \times C}$, labels y, predictions $\hat{y}$
Output: Hub maps h_0 (Control), h_1 (ASMR), FDR-corrected p-values $\hat{p}$
1. Compute class-wise means within each seed:
$\mathsf{Ctrl} = \text{mean}_{\{t:\hat{y}_t = y_t = 0\}} A_t, \quad \mathsf{ASMR} = \text{mean}_{\{t:\hat{y}_t = y_t = 1\}} A_t$
2. Aggregate across seeds:
$\text{Conn}_0 = [\mathsf{Ctrl}^{(1)}, \ldots, \mathsf{Ctrl}^{(R)}]^\top, \quad \text{Conn}_1 = [\mathsf{ASMR}^{(1)}, \ldots, \mathsf{ASMR}^{(R)}]^\top$
3. Threshold and binarize:
For each class k: $t_k = \text{median}(\text{Conn}_k) + \text{std}(\text{Conn}_k)$,
Define $\text{Bin}_k[i, c, j] = \mathbb{I}(\text{Conn}_k[i, c, j] > t_k)$
4. Hub scores:
$H_k[i, c] = \frac{1}{C-1} \sum_j \text{Bin}_k[i, c, j], \quad h_k[c] = \frac{1}{R} \sum_i H_k[i, c]$
5. Statistics:
For each channel c, perform Kruskal-Wallis H-test on $\text{Conn}_0[:, :, c]$ vs. $\text{Conn}_1[:, :, c]$, obtaining p_c.
Apply Benjamini–Hochberg to $\{p_c\} \Rightarrow \hat{p}_c$
return $h_0, h_1, \hat{p}$

where $A \in \mathbb{R}^{N \times N}$, $B \in \mathbb{R}^{N \times F}$, and $C \in \mathbb{R}^{F \times N}$ are learned, u_c is the F-dimensional feature vector for channel c, and x_c its N-dimensional hidden state. By sequentially propagating information across the channel axis, Mamba captures long-range spatial dependencies in a single pass. Both Mamba and the Transformer core modules are followed by position-wise feed-forward layers (with an expansion factor) to enrich their representations [20], [21]. As a reference, we also include two classical baselines—Support Vector Machine and Random Forest classifiers—to benchmark against these deep-learning approaches.

F. Hubness Measure Using Attention Weights

To visualize and interpret the transformer's attention weights, obtained from its core scaled-dot product mechanism, we employed a measure from graph theory called *hubness*. The attention weights allowed us to identify which EEG channels the model focused on to differentiate between classes, which were represented as $C \times C$ matrices for each test subject and were analyzed as follows for hubness computation. Here, *hubness* quantifies how many other channels a given channel is strongly connected to, based on a data-driven suprathreshold criterion: the median of the matrix plus one standard deviation. For each channel, the hubness score was calculated as the proportion of other channels to which it had above-threshold connections—that is, the number of strongly connected channels divided by the total number of channels. We computed hubness measures separately for the ASMR- and ASMR+ groups, and then statistically compared them to identify significant group differences. See Algorithm 1 for detailed computation steps.

G. Training Environment

All analyses were conducted on an NVIDIA RTX A6000 GPU with Python 3.10.13. For machine learning, we employed Leave-One-Subject-Out Cross-Validation (LOSOCV) with five repetitions, using five different random seeds (42, 43, 44, 45, and

TABLE II
SUBJECT-LEVEL PERFORMANCE (MEAN ± SD OVER FIVE SEEDS) OF HFD FEATURES IN CLOSED-EYES CONDITION BETWEEN ASMR- VS. ASMR+; AUCROC IS REPORTED AT THE *SAMPLE* LEVEL

Model	F1 Score	Accuracy	Precision	Recall	AUC ROC
SVM	70.85 ± 0.00	70.97 ± 0.00	71.01 ± 0.00	70.83 ± 0.00	65.47 ± 0.00
Random Forest	73.93 ± 2.42	74.19 ± 2.28	74.59 ± 2.05	73.96 ± 2.36	65.15 ± 1.11
Mamba	77.33 ± 3.98	77.42 ± 3.95	78.10 ± 4.07	77.58 ± 3.96	61.92 ± 2.04
Transformer	$\mathbf{82.56 \pm 3.67}$	$\mathbf{82.58 \pm 3.68}$	$\mathbf{82.64 \pm 3.67}$	$\mathbf{82.58 \pm 3.65}$	$\mathbf{69.80 \pm 0.53}$

46). The hyperparameters for all models were tuned using data from only 10 subjects, five from the ASMR- group and five from the ASMR+ group using grid search from a predefined search space (available on our GitHub Repository).

The best hyperparameters for each model are as follows: For the Transformers model, the optimal hyperparameters found were 50 epochs, a dropout rate of 0.2, weight decay of 0.001, a feedforward expansion of 2, 5 attention heads, and 2 transformer encoder layers, with the AdamW optimizer and GELU activation. The Mamba model had similar settings, with 50 epochs, a dropout rate of 0.2, and weight decay of 0.001, along with a feedforward expansion of 2, a state dimension of 16, 2 Mamba layers, and a convolutional dimension of 5, using the AdamW optimizer with SiLU activation. For the SVM model, the parameters were $C = 0.01$, a polynomial kernel, gamma of 0.1, degree 3, and coef0 of 1.0. For the Random Forest model, the hyperparameters included 50 estimators, a maximum depth of 10, a minimum samples split of 2, a minimum samples leaf of 2, and the square root method for maximum features.

IV. RESULTS

A. Statistical Analysis

We first performed Wilcoxon rank-sum tests at the *regional level* across all frequency bands to examine differences in HFD between brain regions. Subsequently, we conducted Wilcoxon rank-sum tests at the *channel level* within each frequency band to identify specific electrode channels exhibiting significant differences in HFD between the two groups with both open-eye and closed-eye conditions. Our analysis did not yield statistical significance in the closed-eye condition. In open-eyes condition, region-level analysis results, shown in Fig. 2, suggested that in the delta frequency band, Occipital ($p = 0.042$) and Parietal ($p = 0.047$) HFD were significantly greater in the ASMR- compared to the ASMR+ group. A similar trend was observed in the theta band, where frontal ($p = 0.033$), central ($p = 0.013$), and parietal ($p = 0.04$) regions exhibited significantly greater HFD in the ASMR- group compared to the ASMR+ group. In contrast, at the alpha band, an opposite trend was observed, where central ($p = 0.013$), parietal ($p = 0.013$), and temporal ($p = 0.039$) regions exhibited significantly higher HFD in the ASMR+ group compared to the ASMR- group.

To further investigate these effects at the channel level, shown in Fig. 3, we observed that in the delta band, notable differences were found in parietal and occipital channels such as P3, O1, and Oz. In the theta band, significant differences were observed in frontal channels (Fp1, Fp2, and FC2), along with central and parietal channels (Cz, C4, CP1, CP2, CP6, Pz, and P4). In contrast, the alpha band showed differences in channels across multiple regions, including parietal, temporal, frontal, and central regions, with significant effects observed at FC1, FC2, FC6, Cz, C4, T8, CP5, CP1, CP2, CP6, TP10, P7, P3, Pz, and P4.

B. Machine Learning Results

Since the closed-eyes condition did not yield statistically significant effects, the study focused on the open-eyes condition for machine learning classification. Table II and Fig. 5 summarize the performance of four classifiers: two deep-learning architectures (Transformer and Mamba) and two classical machine learning algorithms (SVM and Random Forest). The Transformer achieved the highest F1 score (82.56 ± 3.67), followed by Mamba (77.33 ± 3.98). It also outperformed Mamba in accuracy (82.58 ± 3.68), precision (82.64 ± 3.67), and recall (82.58 ± 3.65). Random Forest and SVM lagged behind, with F1 scores of 73.93 ± 2.42 and 70.85 ± 0.00, respectively. The zero-standard deviation for SVM reflects its deterministic decision boundary, which remains unchanged across random seeds. In terms of misclassification rates for the ASMR+ class, Transformer exhibited the lowest error (17.5%), whereas Mamba showed the highest (27.5%); however, Mamba's misclassification rate for the ASMR- class remained lower than those of Random Forest and SVM. Finally, Transformer also achieved the highest sample-level AUCROC, while Mamba recorded the lowest—underscoring the Transformer's superior discriminative ability between ASMR- and ASMR+ groups.

C. Attention Weights Hubness

To interpret our model's predictions, we employed an explainable AI (XAI) technique that converts transformer attention weights into hubness scores. This analysis uncovered distinct hub patterns that reliably differentiate ASMR- and ASMR+ participants: significant hubs were almost exclusively along a front-to-back midline, spanning frontal, central, parietal, and occipital electrodes, with minimal involvement of temporal channels. Importantly, ASMR+ individuals exhibit significantly weaker hubness proportions (connectivity) than ASMR- (Fig. 4).

V. DISCUSSION

A. HFD Neural Signatures of ASMR

In ASMR+ participants, our resting-state analysis uncovered a distinctive signature of neural complexity. HFD values were significantly lower than those of ASMR- in the delta and theta bands, yet higher in the alpha band, in the eyes open resting state condition. This pattern points to an altered baseline mode of visual processing in the ASMR+ individuals. In contrast, conventional power analyses (included on GitHub) showed only significant differences in the beta band at frontal ($p = 0.035$), central ($p = 0.005$), temporal ($p = 0.035$), and parietal ($p = 0.042$) regions. Taken together, these results demonstrate that HFD is markedly more sensitive than PSD—particularly in the

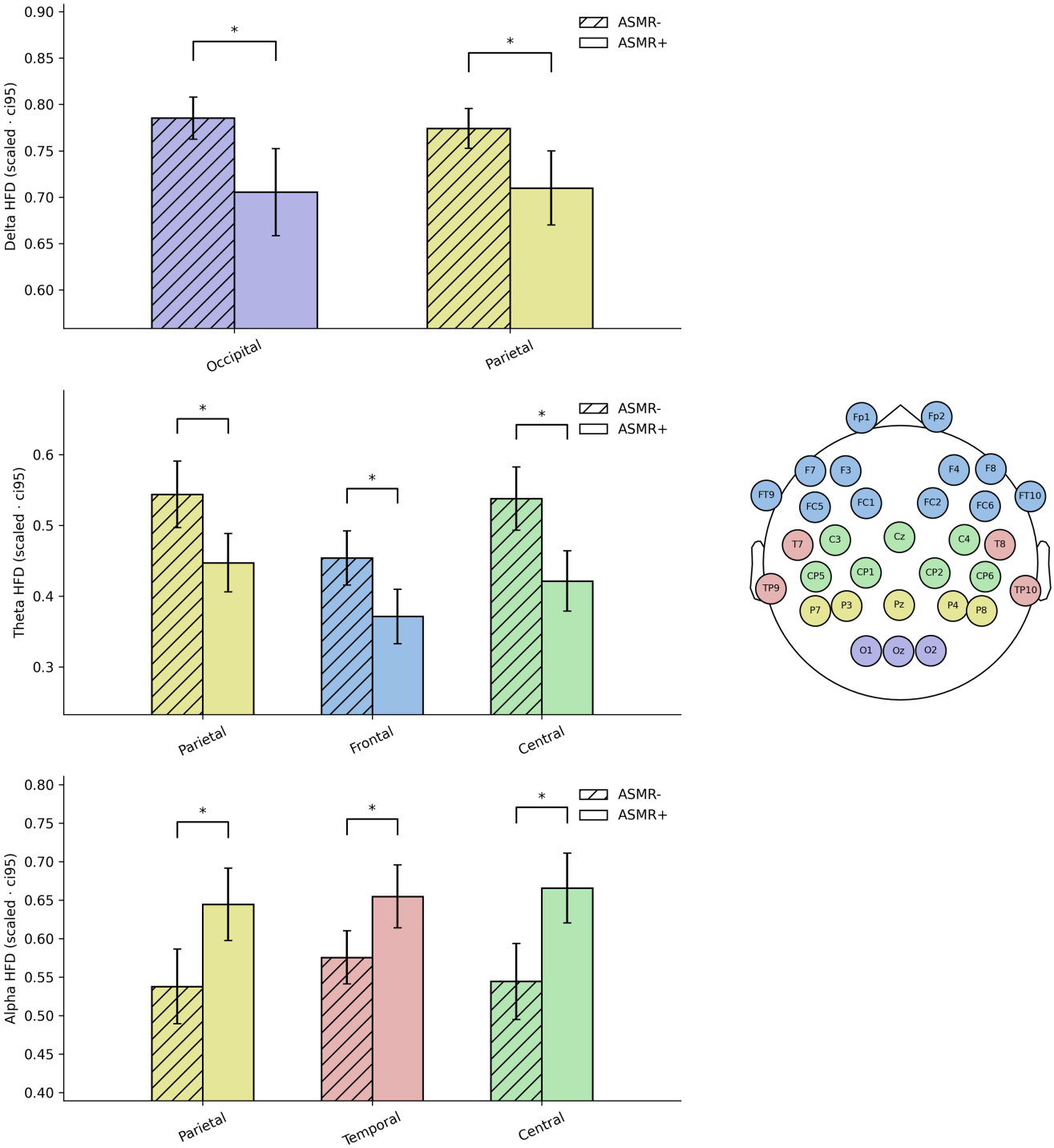

Fig. 2. Difference in mean HFD between ASMR- and ASMR+ participants during resting state open-eyes condition. Pairwise comparisons were made between ASMR- (diagonal lines) and ASMR+ (no pattern) participants for each region, electrode group and frequency bands. The location of electrodes that comprise each group is indicated in the topographic map by the corresponding colour. $* \; p < 0.05$.

eyes-open condition—for detecting subtle, frequency-specific complexity differences between ASMR- and ASMR+ groups.

These resting-state complexity changes echo previous stimulus-driven findings. For instance, Mohammadi et al. [8] reported a global decrease in delta and theta power during ASMR stimulus exposure, linking it to increased relaxation, while other previous work [7], [22], [23] showed elevated frontal-lobe alpha activity tied to attentional and sensorimotor engagement. Importantly, by using HFD instead of PSD, we detect these same frequency-specific alterations *without* any external stimulus. This shows that fractal complexity is a powerful, resting-state marker of ASMR brain dynamics. Moreover, our xAI analysis results, using and converting transformer attention weights into hubness scores, align with resting-state fMRI findings by Smith

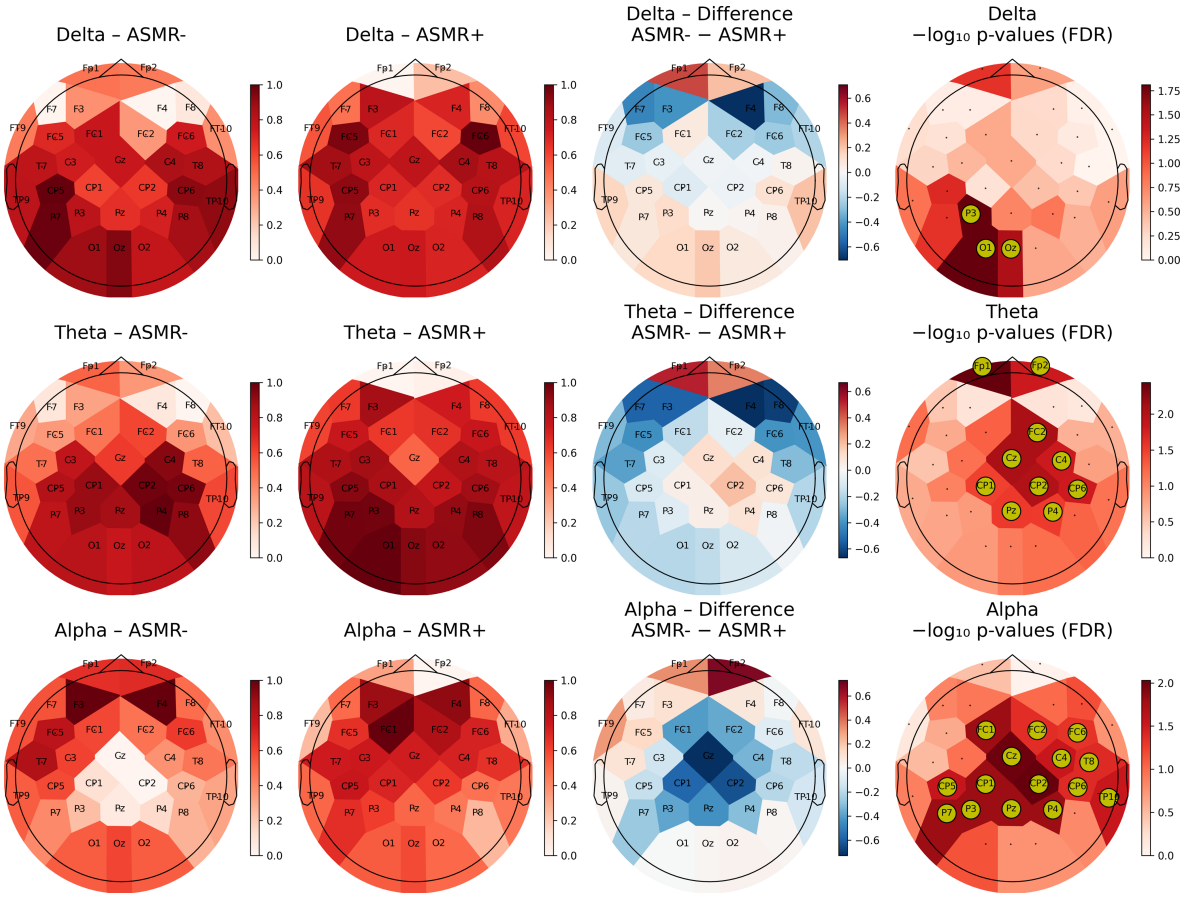

Fig. 3. Topographic maps of HFD in the Open-Eyes condition for ASMR- and ASMR+ groups across three EEG frequency bands. Each row corresponds to one band— delta (δ), theta (θ), and alpha (α), —from top to bottom. Columns show (1) group-mean HFD for ASMR- subjects, (2) group-mean HFD for ASMR+ subjects, (3) the pointwise difference, and (4) FDR-corrected q-values with significant electrodes (q $<$ 0.05) marked by yellow circles.

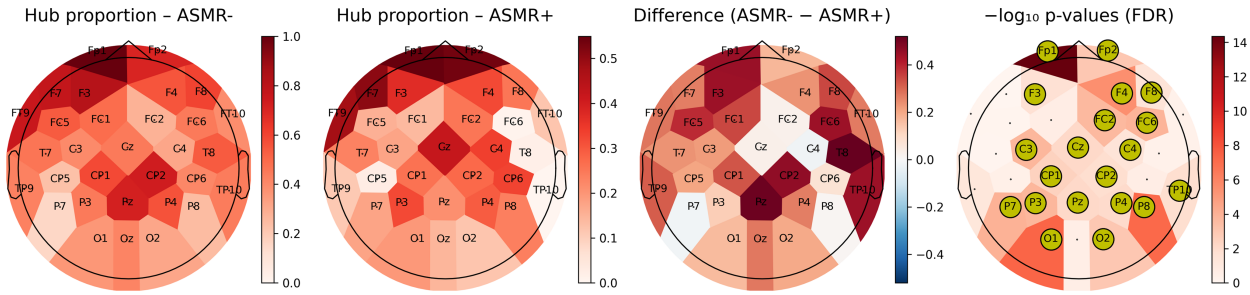

Fig. 4. Topographic maps of attention weights from the transformer model in the open-eyes condition for the ASMR- and ASMR+ groups.

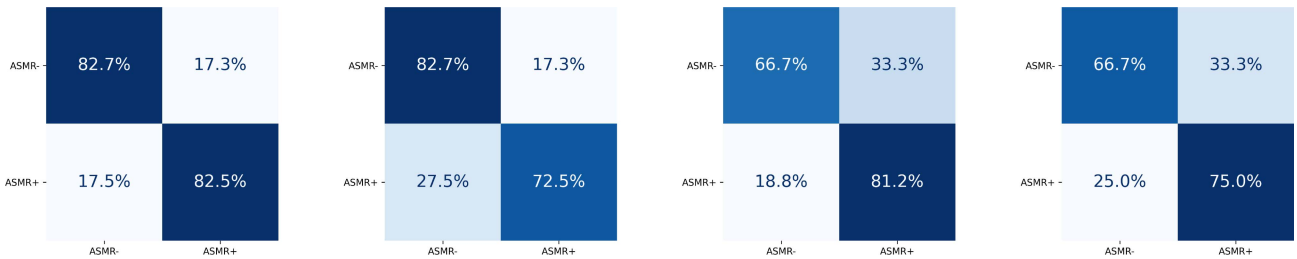

(a) Transformer (b) Mamba (c) Random Forest (d) SVM

Fig. 5. Confusion matrices of subjectlevel predictions in percentage format across five random seeds for each model.

et al. [14], who reported reduced default mode network connectivity in ASMR+ individuals. Consistent with this, our model uncovers significantly weaker hubness connectivity in ASMR+ participants compared to ASMR-.

B. Supplement to Therapeutic Approaches

ASMR reliably induces a relaxation state in ASMR+ individuals, suggesting its potential as a supplement to conventional therapies. However, one might ask why clinicians cannot simply rely on self-report—e.g., "Do you experience ASMR tingles?"—rather than employ EEG. Although convenient, such subjective screening is prone to demand characteristics and recall bias. By contrast, we identified an objective marker from a brief, stimulus-free resting-state EEG: HFD complexity. A transformer classifier trained on HFD features from eyes-open recordings distinguished ASMR- participants from ASMR+ with 82.58% accuracy and 82.50% recall, showing that resting-state complexity alone captures the neural signature of ASMR sensitivity.

Importantly, a key limitation of the current work is that the model predicts only binary group membership rather than the intensity of the relaxation response. Future research should extend both the experimental design and the AI models to a multi-class (ASMR- Vs ASMR+), multi-label (relaxation intensity) framework by integrating pre- and post-EEG questionnaires or subjective tingling ratings. Such integration would allow simultaneous prediction of ASMR sensitivity and the magnitude of the relaxation effect, moving ASMR-based AI models closer to real-world therapeutic applications. We further note that our study analyzed data from only 31 subjects; this modest sample size may limit generalizability and therefore warrants cautious interpretation. Although the machine learning was performed segment-wise (540 ten-second segments), these segments are not independent observations of different subjects. Leave-one-subject-out cross-validation (LOSOCV) reduces the risk of data leakage between training and test sets but does not substitute for validation on larger, independent cohorts. Consequently, our results should be viewed as preliminary and require replication in larger, external datasets. Nonetheless, the segment-level analysis provides additional statistical power and a useful reference for future ASMR and EEG complexity studies employing machine-learning methods.

VI. Conclusion

The purpose of this study was to examine whether ASMR sensitivity is associated with baseline differences in neural activity during eyes-open and eyes-closed resting-state conditions. HFD uncovered distinct, frequency-specific alterations. ASMR+ individuals showed reduced complexity in the delta and theta bands, consistent with a more relaxed baseline state, and increased complexity in the alpha band, indicative of heightened alertness and attentional readiness. These results show that HFD is a more sensitive marker than PSD for detecting subtle resting-state neural differences linked to ASMR sensitivity.

References

[1] E. L. Barratt and N. J. Davis, "Autonomous sensory meridian response (asmr): A flow-like mental state," *PeerJ*, vol. 3, 2015, Art. no. e851.

[2] G. L. Poerio, E. Blakey, T. J. Hostler, and T. Veltri, "More than a feeling: Autonomous sensory meridian response (ASMR) is characterized by reliable changes in affect and physiology," *PLoS One*, vol. 13, no. 6, 2018, Art. no. e0196645.

[3] B. Fredborg, J. Clark, and S. D. Smith, "An examination of personality traits associated with autonomous sensory meridian response (ASMR)," *Front. Psychol.*, vol. 8, 2017, Art. no. 247.

[4] S. D. Smith, B. K. Fredborg, and J. Kornelsen, "Atypical functional connectivity associated with autonomous sensory meridian response: An examination of five resting-state networks," *Brain Connectivity*, vol. 9, no. 6, pp. 508–518, 2019.

[5] G. L. Poerio, M. Ueda, and H. M. Kondo, "Similar but different: High prevalence of synesthesia in autonomous sensory meridian response (ASMR)," *Front. Psychol.*, vol. 13, 2022, Art. no. 990565.

[6] UCLA Health (2023), "Large portion of the population may feel ASMR benefits," Accessed: Apr. 8, 2025.

[7] B. K. Fredborg, K. Champagne-Jorgensen, A. S. Desroches, and S. D. Smith, "An electroencephalographic examination of the autonomous sensory meridian response (ASMR)," *Consciousness Cogn.*, vol. 87, 2021, Art. no. 103053.

[8] A. Mohammadi, S. Seifzadeh, F. Torkamani, and S. Salehi, "An experimental eeg study of brain activities underlying the autonomous sensory meridian response," *IBRO Neurosci. Rep.*, vol. 18, pp. 6–15, 2025.

[9] H. Engelbregt, K. Brinkman, C. V. Geest, M. Irrmischer, and J. B. Deijen, "The effects of autonomous sensory meridian response (ASMR) on mood, attention, heart rate, skin conductance and EEG in healthy young adults," *Exp. Brain Res.*, vol. 240, no. 6, pp. 1727–1742, 2022.

[10] Y. Ohta and K. Inagaki, "Evaluation of the effect of ASMR on reduction of mental stress: Eeg study," in *Proc. IEEE 3rd Glob. Conf. Life Sci. Technol.*, 2021, pp. 88–89.

[11] R. Tan, H. Shoenberger, W. Cong, and M. Mahdavi, "Understanding the structural components behind the psychological effects of autonomous sensory meridian response (ASMR) with machine learning and experimental methods," *J. Media Psychol.*, vol. 35, no. 3, pp. 181–189, 2023.

[12] J.-Y. Moon, "DeepASMR: A deep learning–based ASMR platform," Ph.D. thesis, Graduate School of Seoul National University, Seoul, South Korea, 2021.

[13] T. Higuchi, "Approach to an irregular time series on the basis of the fractal theory," *Physica D: Nonlinear Phenomena*, vol. 31, no. 2, pp. 277–283, 1988.

[14] S. D. Smith, B. Katherine Fredborg, and J. Kornelsen, "An examination of the default mode network in individuals with autonomous sensory meridian response (ASMR)," *Social Neurosci.*, vol. 12, no. 4, pp. 361–365, 2017.

[15] B. C. Lochte, S. A. Guillory, C. A. Richard, and W. M. Kelley, "An FMRI investigation of the neural correlates underlying the autonomous sensory meridian response (ASMR)," *BioImpacts: BI*, vol. 8, no. 4, 2018, Art. no. 295.

[16] S. D. Smith, B. K. Fredborg, and J. Kornelsen, "A functional magnetic resonance imaging investigation of the autonomous sensory meridian response," *PeerJ*, vol. 7, 2019, Art. no. e7122.

[17] E. Shamsi, M. A. Ahmadi-Pajouh, and T. S. Ala, "Higuchi fractal dimension: An efficient approach to detection of brain entrainment to theta binaural beats," *Biomed. Signal Process. Control*, vol. 68, 2021, Art. no. 102580.

[18] K. Gladun, "Higuchi fractal dimension as a method for assessing response to sound stimuli in patients with diffuse axonal brain injury," *Nat. Center Biotechnol. Inf.*, vol. 12, no. 4 (ENG), pp. 63–70, 2020.

[19] I. Winkler, S. Debener, K.-R. Müller, and M. Tangermann, "On the influence of high-pass filtering on ICA-based artifact reduction in EEG-ERP," in *Proc. 37th Annu. Int. Conf. IEEE Eng. Med. Biol. Soc.*, 2015, pp. 4101–4105.

[20] A. Vaswani et al., "Attention is all you need," in *Proc. Adv. Neural Inf. Process. Syst.*, 2017, vol. 30, pp. 1–11.

[21] A. Gu and T. Dao, "Mamba: Linear-time sequence modeling with selective state spaces," 2023, *arXiv:2312.00752*.

[22] K. Inagaki and Y. Ohta, "Capacity of autonomous sensory meridian response on the reduction of mental stress," *Int. J. Environ. Res. Public Health*, vol. 19, no. 21, 2022, Art. no. 14577.

[23] N. Sakurai, K. Nagasaka, S. Takahashi, S. Kasai, H. Onishi, and N. Kodama, "Brain function effects of autonomous sensory meridian response (ASMR) video viewing," *Front. Neurosci.*, vol. 17, 2023, Art. no. 1025745.